Journal of Materials Chemistry C
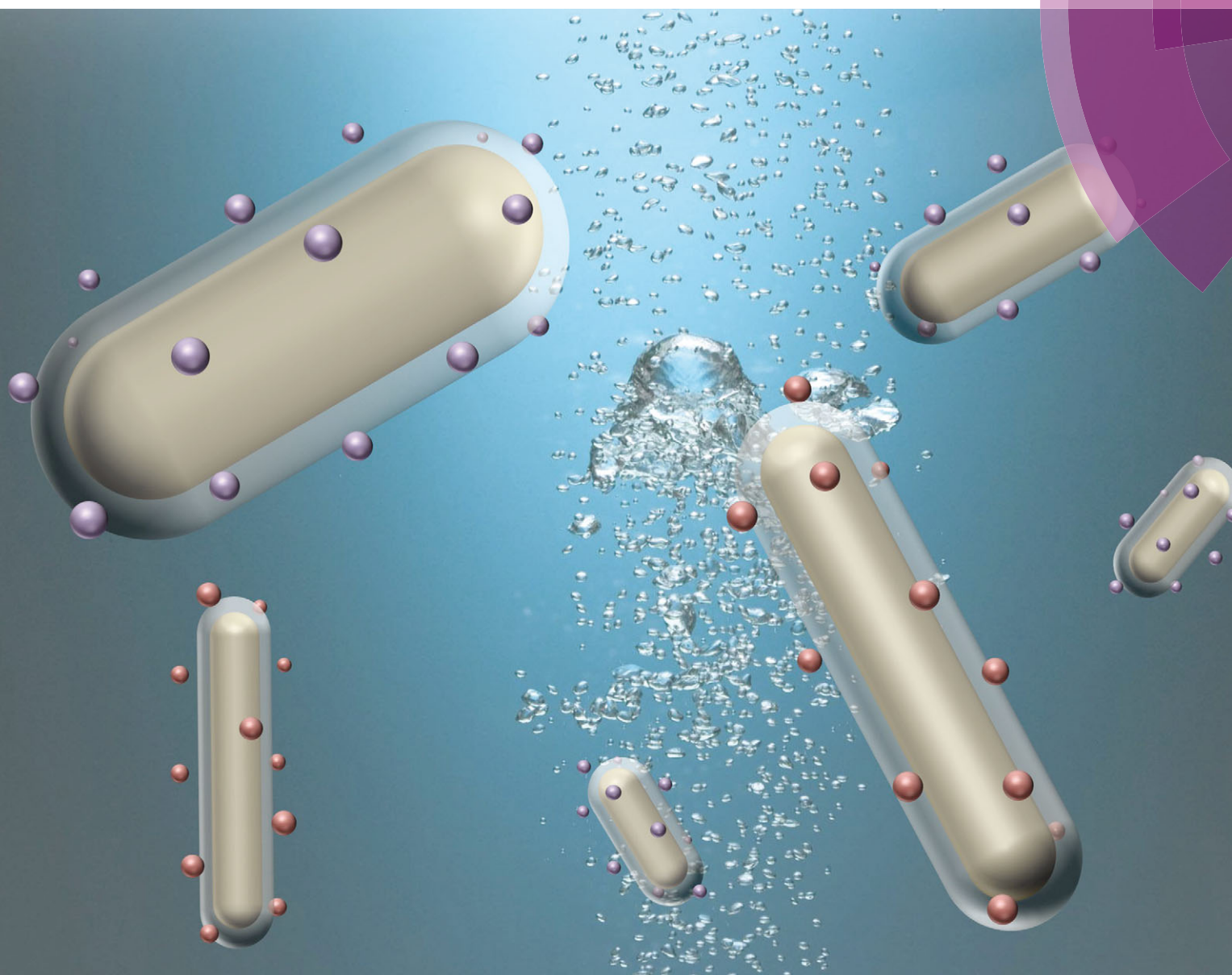
Materials for optical, magnetic and electronic devices

www.rsc.org/MaterialsC

ROYAL SOCIETY
OF CHEMISTRY

PAPER
Nguyễn T. K. Thanh, Xiaodi Su *et al.*
Fine-tuning of gold nanorod dimensions and plasmonic properties using the Hofmeister effects

175 YEARS

PAPER

CrossMark
← click for updates

Fine-tuning of gold nanorod dimensions and plasmonic properties using the Hofmeister effects†

Roger M. Pallares,[ab] Xiaodi Su,*[b] Suo Hon Lim[b] and Nguyễn T. K. Thanh*[cd]

Gold nanorods (Au NRs) present unique optical and electronic properties that depend on their morphology. Their applications in sensing and therapeutics require easy synthesis with precise control over their dimensions. Here, we report a method for the synthesis of highly pure and monodisperse Au NRs with fine-tuneable dimensions and longitudinal localised surface plasmon resonance by addition of Hofmeister salts into the growth medium. The control of Au NR formation relies on the double interaction between salt–gold and salt–surfactant (cetyl trimethylammonium bromide, CTAB). With the addition of Hofmeister salts (*i.e.* $NaNO_3$, $NaBr$, $NaCl$ and $NaHSO_4$) we can fine-tune the aspect ratio of Au NRs in the range of 3.3 to 4.8 with a precision of 0.1 and the longitudinal absorption band from 777 to 960 nm. In addition, we have studied the physical changes in the CTAB micelles induced by the salts using rheology, electron microscopy and light-scattering techniques. We report for the first time cryo-electron microscopy imaging of the micelles under Au NR growth conditions. With the comprehensive characterization of CTAB micelles in the growth solution, this study provides a deeper understanding of the anisotropic growth of metallic crystals.

[a] *Department of Chemistry, University College London, London, WC1H 0AJ, UK.*
   E-mail: ntk.thanh@ucl.ac.uk
[b] *Institute of Materials Research and Engineering, A*STAR (Agency for Science, Technology and Research), 3 Research Link, Singapore, 117602, Singapore. E-mail: xd-su@imre.a-star.edu.sg*
[c] *UCL Healthcare Biomagnetic and Nanomaterials Laboratories, 21 Albemarle Street, London W1S 4BS, UK*
[d] *Biophysics Group, Department of Physics and Astronomy, University College London, London, WC1E 6BT, UK*

† Electronic supplementary information (ESI) available: A summary of Hofmeister salts added to the growth solutions; the optical and morphological properties of synthesized Au NRs and the relative viscosities of all growth solutions. See DOI: 10.1039/c5tc02426a

Introduction

Over the past decade the nanoplasmonic field has been significantly developed due to the introduction of a variety of novel synthetic methods and biofunctionalisation strategies for new morphologies beyond the sphere (*i.e.* nanorod, nanostar, nanocross, *etc.*).[1] Anisotropic plasmonic nanoparticles have been the subject of numerous studies because of their unique optical and electronic properties, *e.g.* strong absorbance in the near-infrared region,[2] higher incoupling efficiency[3] or a significant increase in the surface-enhanced Raman spectroscopy signal.[4] Among different nanocrystals, gold nanorods have attracted great attention because of their distinct nanoplasmonic properties and successful utilization in a wide range of biological applications such as photothermal therapy,[5–8] drug delivery,[9] imaging[10–13]

and sensing.[14–16] One of their main features is the longitudinal localised surface plasmon resonance (L-LSPR), the light-induced coherent collective oscillation of the valence electrons through the longitudinal axis, which results in a unique and intense light absorption in a wide wavelength range.[17,18] This optical property depends highly on the aspect ratio of the rod that can be customised through the controlled synthesis.

The most common synthesis of Au NRs is the seed-mediated method, which was initially developed by Murphy *et al.*[19] and later improved by El-Sayed *et al.*[20] This seed-mediated method is a two-step procedure. Firstly, gold seeds are obtained by the fast reduction of gold salts by $NaBH_4$. Subsequently, the obtained gold seeds are used as nucleation points for the slow reduction of the gold salts by ascorbic acid in the presence of CTAB surfactant. Interestingly, depending on the nature and structure of the seeds, different kinds of Au NRs can be obtained. Initially, Murphy *et al.* used citrate-capped penta-twinned gold nanoparticles as seeds, which yielded twinned crystal rods with {111} faces (silverless synthesis). On the other hand, El-Sayed *et al.* synthesized the seeds in the presence of CTAB,[20] yielding single crystal nanoparticles of 1.5 nm diameter.[21] Those seeds were later used to grow single crystal Au NRs in the presence of $AgNO_3$ (silver assisted synthesis). The exact role of CTAB in the promotion of the anisotropic growth is still unclear. At early stages, El-Sayed *et al.* suggested that CTAB acted as a soft template.[20] However, subsequent publications indicated the CTAB adsorption onto specific gold facets, favouring specific surface passivation.[22,23] Furthermore, the shape-sensitivity

to CTAB impurities,[24] the presence of halides[25,26] and the temperature effect[27,28] were also reported. A big effort has recently been made in order to enhance the tunability and monodispersity of Au NRs. Murray *et al.* reported a synthesis with high control over the nanocrystal growth through the inclusion of aromatic additives, which changed the micellar packing of the surfactant.[29] In addition, alternative reducing agents[30,31] or different surfactants[32,33] have also been used to increase the quality of the Au NRs.

Interestingly, CTAB molecules self-assemble into spheroid shaped micelles in water.[34] The addition of salts, co-surfactants or other additives can change the micellar behaviour, *e.g.* transition from sphere to rod or worm-shaped micelles.[35] In the presence of salts, the changes in micelles are caused by the screening of the electrostatic repulsion between the polar heads of the surfactant molecules. A comparison between the effects of different anions on micellar growth showed that they follow the Hofmeister series order,[36] which is a historical classification of salt capacity to precipitate proteins in water. The protein precipitation is affected by the electrostatic forces of the ions and their capacity to affect the surrounding water structure.[37] Traditionally, the anionic order of the Hofmeister series has been considered as the following: $SCN^- > ClO_4^- > I^- > ClO_3^- > NO_3^- > Br^- > Cl^- > HSO_4^- > SO_4^{2-}$.

In this work, we present a new methodology to fine-tune the Au NRs while keeping the well-established seed-mediated synthesis as a basis. As mentioned earlier, the customisation of monodisperse Au NRs has been generally achieved by using alternative reducing agents, co-surfactants or organic additives. In our method, we successfully employed a fourth strategy: the use of Hofmeister salts, which provide precise control over the morphology and optical properties of the crystals. Moreover, for the first time, the CTAB micelle morphology has been studied under Au NR growth conditions, yielding new insights on the anisotropic growth of rods.

Experimental section

Materials

The following products were used as received. Sodium nitrate ($NaNO_3$, >99%), sodium bromide (NaBr, >99%), sodium chloride (NaCl, >99%), sodium bisulfate ($NaHSO_4$, >99%), sodium thiocyanate (NaSCN, >98%), sodium perchlorate ($NaClO_4$, >98%), hydrogen tetrachloroaurate trihydrate ($HAuCl_4·3H_2O$), silver nitrate ($AgNO_3$, 0.1 N), hydrogen chloride (HCl, 37 wt% in water), L-ascorbic acid (crystalline), and sodium borohydride ($NaBH_4$, 98%) were purchased from Sigma-Aldrich. Hexadecyltrimethylammonium bromide (CTAB, >98%) was purchased from Tokyo Chemical Industry.

All the water employed in the experiments was obtained using a Milli-Q Integral 5 system. All glassware was cleaned with aqua regia, rinsed extensively with water, and dried before use.

Synthesis of Au NRs

Synthesis of seeds. The reaction was performed at 22 °C. The CTAB solution (5 mL, 0.2 M) was added to a 5.0 mL solution of 0.5 mM $HAuCl_4$. While the mixture was being vigorously stirred, 0.6 mL of 10 mM ice-cold $NaBH_4$ was added at once. The seed solution was stirred for 30 s and was left undisturbed for 30 min. Then, the seeds were immediately used to synthesize the gold nanorods. Fresh seeds are necessary to obtain monodisperse Au NRs,[38] with most synthetic procedures letting the seeds age between 30 min and 2 h.[22,29,32,33] In addition, CTAB solubility in water is 0.1 M at 20 °C.[39] Thus, the shorter the aging time is, the less likely CTAB is to start precipitating.

Synthesis of rods. 250 μL of $AgNO_3$ (4 mM) were added to 5.0 mL solution of CTAB (0.1 M). The solution was kept undisturbed for 15 min, after which 5 mL of $HAuCl_4$ (1 mM), a specific volume of one of the salt solutions (Table S1, ESI†) and 12 μL of HCl (37%) were added. After slow stirring, ascorbic acid (75 μL, 79 mM) was introduced into the growth solution, which lost its orange colour and yielded a colourless solution, because of the reduction of Au^{3+} to Au^{1+}. The mixture was vigorously stirred for 30 s and 60 μL of the seed solution were added. Finally, the growth solution was vigorously stirred for 30 s and left undisturbed for 12 h. The gold nanorods were isolated by centrifugation at 8000 rpm for 15 min followed by removal of the supernatant twice. The precipitate was re-dispersed in 10 mL of Milli-Q water. It is noteworthy to mention that the stoichiometric ratio between $HAuCl_4$ and ascorbic acid is 1 : 1.5 in the gold reduction reaction.[40] However, this ratio presents fast reaction kinetics, which yields short[41] and not well monodispersed rods. Due to the fact that we prioritize monodispersity over yield, the 1 : 1.2 ratio was used with a maximum yield of 80%. Previous researchers have used the same ratio[42] or even lower.[29,32]

Characterization

Transmission electron microscopy (TEM) images were acquired using a JEM-1010 microscope operating at 100 kV. High-resolution transmission electron microscopy (HR-TEM) images were obtained using a JEM-2100 microscope operating at 200 kV. Cryo-transmission electron microscopy (cryo-TEM) imaging was performed using a Titan Krios cryo-TEM operating at 300 kV. The study of the nanoparticle and micelle morphology and size distribution was performed by analysing several TEM, HR-TEM or cryo-TEM images obtained for every sample. The optical extinction spectra were recorded using a Spectramax M2/M2^e UV/Vis/NIR spectrophotometer. The dynamic light scattering (DLS) and zeta-potential measurements were performed using a Zetasizer Nano Z from Malvern Instruments. The X-ray diffraction (XRD) measurements were performed using a D8 Discover Gadds. The viscosity data were obtained using a Cannon-Fenske viscometer.

Results and discussion

Tuning the L-LSPR band

Even though the exact mechanism involved in the Hofmeister series is not clear, it is widely accepted that the series can be

divided into different sections depending on their salting-in/salting-out effects.[43] The first group includes ions with small hydrated radii and salting-out capacities (*e.g.* NH_4^+ or F^-). Following is a group with neutral or moderate behaviour (*e.g.* Cl^- or Na^+). Finally, the last group is composed of bigger ions with lower ionic strength, which present the salting-in effect (*e.g.* SCN^- or Ca^{2+}).

In order to explore the tuning capacities of Hofmeister anions, the following six salts were studied: NaSCN, NaClO$_4$, NaNO$_3$, NaBr, NaCl and NaHSO$_4$. Na$^+$ was selected to be present in all the salts in order to have an equalised cationic effect in all the experiments. All the anions were monovalent and representatives of the Hofmeister series. SCN^- and ClO_4^- present the salting-in ability; NO_3^-, Br^- and Cl^- are neutral members of the series and HSO_4^- has the salting-out capacity.

As described in the Experimental section, Au NRs were synthesised using our own modified version of seed-mediated method,[20] by introducing the selected salts at different concentrations (Table S1, ESI†) in the growth solution before the addition of ascorbic acid. The extinction spectra of the resulting Au NRs with NaNO$_3$, NaCl, NaHSO$_4$ and NaBr are plotted in Fig. 1. It is important to note that the growth solution contains some Hofmeister anions from the beginning, such as bromide (from CTAB), nitride (from AgNO$_3$) and chloride (from HCl). However, their concentrations are the same in all samples, therefore their effects are equal in all the cases. The values shown in the text and figures are the added concentrations of Hofmeister salts.

Among the six tested anion salts, SCN^- and ClO_4^- quenched the reduction reaction of gold salt and precipitated the surfactant. The colour change in the growth solution from colourless to red, which indicates Au NR formation, was not observed. These observations were in agreement with previous studies, which showed a decrease in the reduction potential of gold ions after their conjugation with SCN^- [44] and aggregation of dodecyltrimethylammonium bromide (cationic surfactant with 12 aliphatic carbons instead of 16 like CTAB) induced by SCN^- and its precipitation by ClO_4^-.[45] The rest of the four salts did allow the synthesis of Au NRs and more importantly tuned the L-LSPR band either to longer or shorter wavelengths.

NaNO$_3$, NaCl and NaHSO$_4$ red-shifted the L-LSPR band, with bigger changes coming from the addition of 50 mM NaNO$_3$ (Δ_{L-LSPR} = 76 nm). The addition of 50 mM NaCl or 50 mM NaHSO$_4$ produced similar effects with Δ_{L-LSPR} up to 44 and 49 nm, respectively. NaBr had the biggest impact on the L-LSPR peak, *i.e.* blue-shifting it up to 107 nm from the lowest to the highest salt concentration. In contrast to the other salts, the maximum concentration of the added NaBr in the growth solution was 30 mM, above this amount spheroid shape particles were mainly obtained. It is worth mentioning that the low intensity of the bands at around 510 nm indicates the high shape purity of the samples.

Finally, since Hofmeister series only include few representatives, the behaviour of other ions can be estimated by comparing their hydrated radii and salting-in or salting-out abilities with the ions contained in the series. This can be used as a tool for predicting the influence of salts on the growth of Au NRs.

Morphology and crystalline structure of the Au NRs

Fig. 2 shows the TEM images of the monodisperse Au NRs with small shape impurities (average below 6%) obtained by our modified El-Sayed synthesis. As expected, the variations in the aspect ratios are coherent with the shifts of the L-LSPR band induced by the salts (Table S2, ESI†). Therefore, NaNO$_3$ (0–50 mM) leads to the biggest increase in the aspect ratio from 4.1 up to 4.8. NaCl and NaHSO$_4$ (0–50 mM) lead to a similar increase in the aspect ratio of up to 4.7 and 4.6, respectively. On the other hand, NaBr (0–30 mM) leads to a decrease of the aspect ratio from 4.1 to 3.3.

Interestingly, the increase of the aspect ratio linked to NaNO$_3$ is mainly caused by the reduction of the rod widths (from 10.6 nm to 8.8 nm), but to a little extent by rod elongation (no clear tendency of elongation), as shown in Table S2 (ESI†). The increase in aspect ratios caused by NaCl and NaHSO$_4$ is due to both the elongation (up to 45.6 and 45.0 nm final lengths, respectively, at the highest salt concentration) and the width reduction (down to 9.8 nm for both salts) of the rods at the same time. On the other hand, the addition of NaBr to
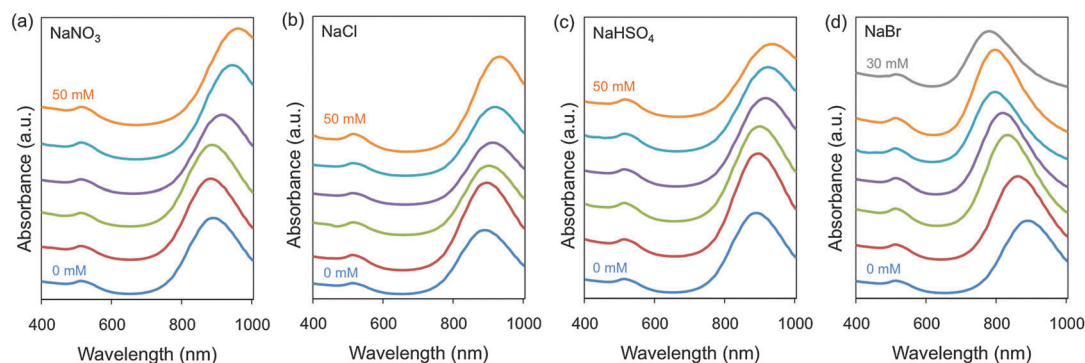

Fig. 1 Normalized extinction spectra of Au NRs grown in the presence of additional amounts of Hofmeister salts. For (a)–(c) the salt concentrations are 0 mM (blue), 10 mM (red), 20 mM (green), 30 mM (purple), 40 mM (turquoise) and 50 mM (orange) from bottom to top. For (d), the salt concentrations are 0 mM (blue), 5 mM (red), 10 mM (green), 15 mM (purple), 20 mM (turquoise), 25 mM (orange) and 30 mM (grey) from bottom to top. All the spectra have been offset for easier comprehension.
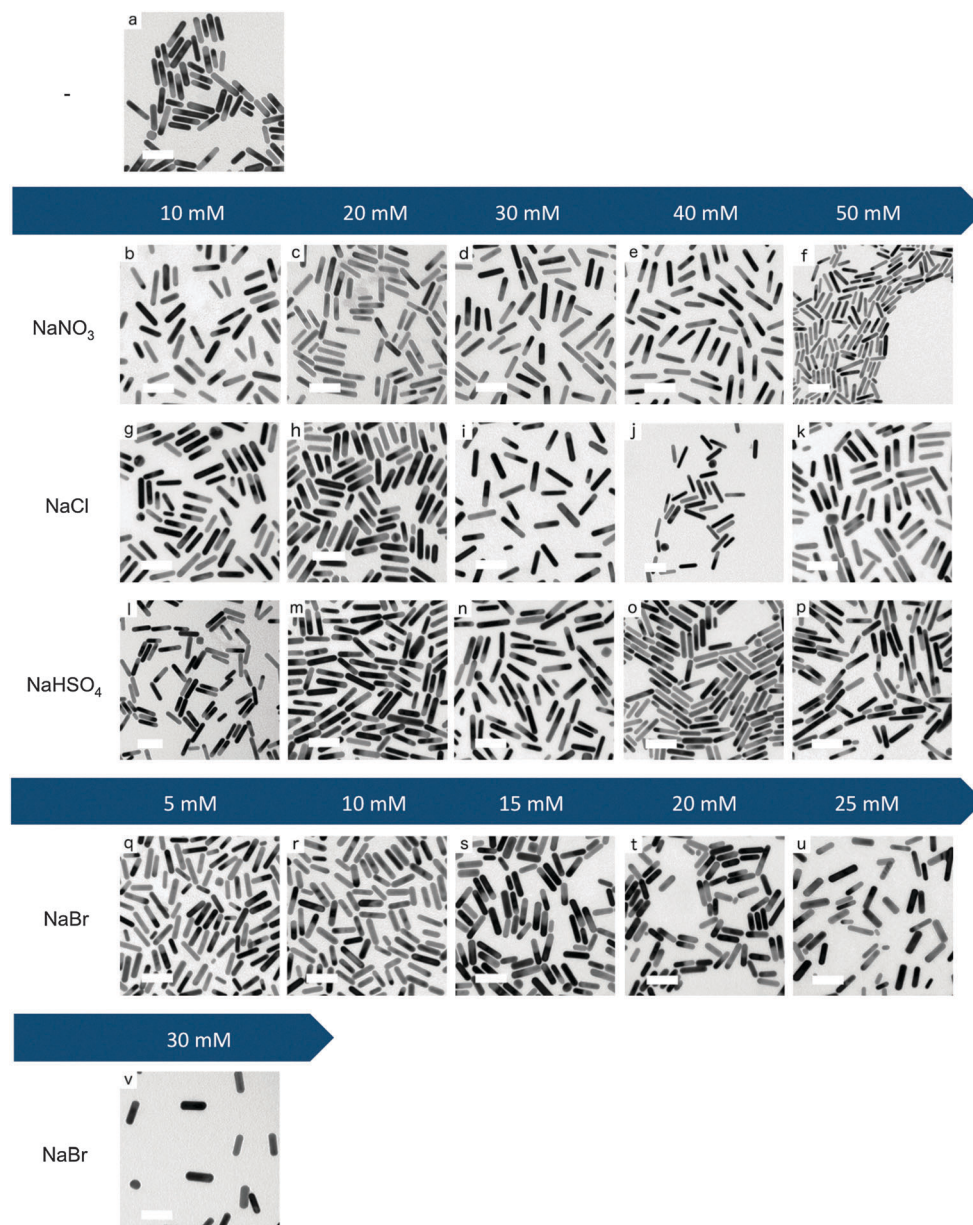
Fig. 2 TEM images of Au NRs synthesized using our seed-mediated method with different amounts of Hofmeister salts: (a) without Hofmeister salts, (b–f) with NaNO₃, (g–k) with NaCl and (l–p) with NaHSO₄ in the order of increasing added concentration (10–50 mM), and (q–v) with NaBr in the order of increasing added concentration (5–30 mM). All scale bars are 50 nm.

the growth solutions yields shorter and wider rods from 43.0 × 10.6 nm to 36.8 × 11.2 nm, resulting in lower aspect ratio crystals. The statistical significance of different aspect ratios was studied by Welch's t-tests (Table S3, ESI†) and effect-size calculations (Table S4, ESI†). These show that with our method the aspect ratio of the rods can be fine-tuned with a precision of 0.1 for most of the range between 3.3 and 4.8 with small effect-sizes ($0.1 < d < 0.2$) but with statistical significance ($p < 0.05$).

In addition, we studied the crystalline structure of Au NRs through HR-TEM and XRD analyses. The fast Fourier transform patterns of all the samples show face centered cubic (fcc) close packing, examined along the [110] zone axis (Fig. 3).[46] HR-TEM data prove that the Au NRs are single-crystals. Furthermore, it is

clear that the rods grow along the [001] direction. Fig. 4 shows the XRD patterns of the samples obtained with the maximum amount of Hofmeister salts. In all the cases the XRD peaks are coherent with the metallic gold where the strongest peaks are (111) and (200).[47]

Evolution of CTAB micelles

To clarify the role of CTAB in the synthesis of Au NRs, it is necessary to characterize the evolution of the CTAB micelles under different growth conditions. The immiscibility between the aliphatic chain of CTAB and water induces their aggregation in cationic sphere-shaped micelles. It is well established that the electrostatic interactions between the surfactant polar
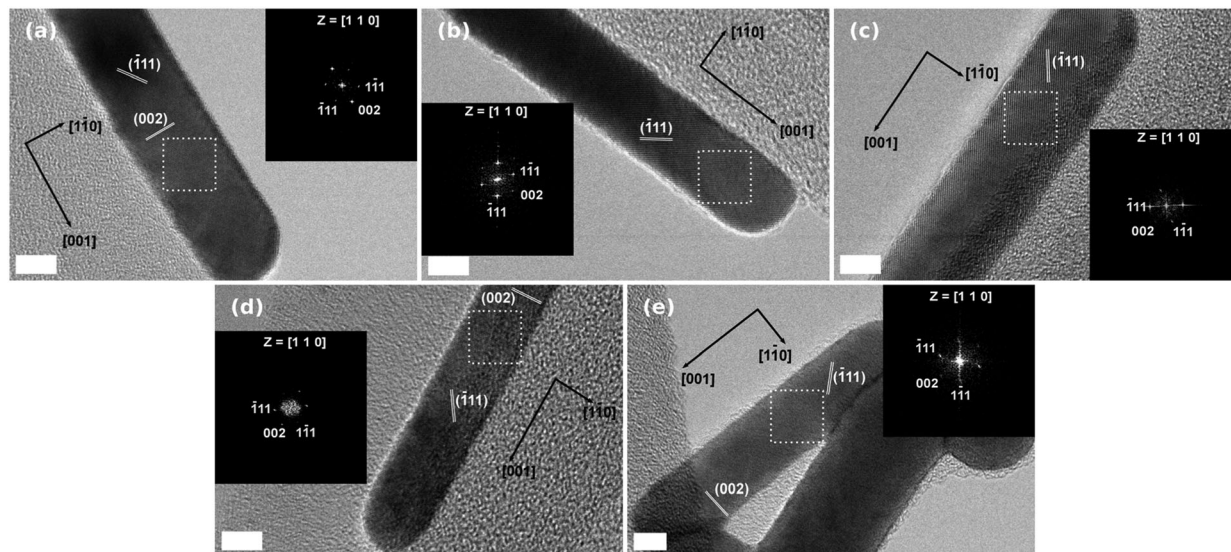
Fig. 3 HR-TEM images of Au NRs synthesized (a) without Hofmeister salts, (b) with $NaNO_3$ (50 mM), (c) with NaCl (50 mM), (d) with $NaHSO_4$ (50 mM) and (e) with NaBr (30 mM). The insets in the images are the fast Fourier transform patterns of the selected regions. All scale bars are 5 nm.
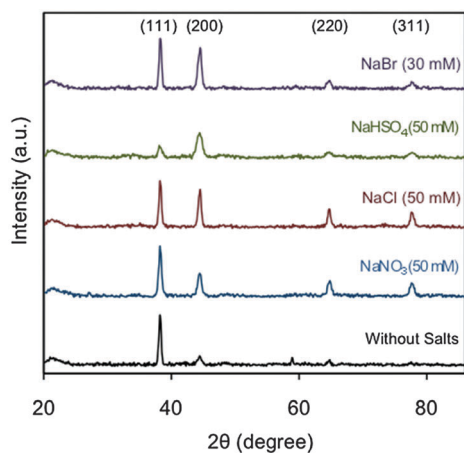

Fig. 4 XRD patterns of Au NRs obtained with and without added Hofmeister salts.

heads and the charged species modify the micelle zeta potential,[48] which has been suggested to play an important role in the growth of Au NRs.[28] Fig. 5a depicts the electrokinetic potential of CTAB

micelles in the growth solution after the addition of different Hofmeister salt concentrations. The initial value without added Hofmeister salts is 43.5 mV and it linearly decreases with $NaNO_3$, NaCl and NaBr down to 31.1, 33.7 and 37.0 mV, respectively. Interestingly, $NaHSO_4$ is the salt that most reduces the micelle zeta potential, down to 27.9 mV.

The interaction between the salts and the CTAB micelles also results in the screening of the electrostatic repulsion between the surfactant polar heads, which alters the surfactant packing and can trigger morphological transitions,[34] such as spherical-to-wormlike micelle transitions. The micelle morphologies have been mainly characterized by three different kinds of techniques: linear rheology, cryo-TEM and scattering based methods, as they have been deeply discussed in a recent review article.[34] Fig. 5b presents the CTAB micelle hydrodynamic diameter (D_H) in the growth solution as a function of increasing salt content as measured by dynamic light scattering (DLS). The D_H increased in all the samples and was proportional to both the salt concentration and the position of the anion in the Hofmeister series, suggesting that the salt triggers the micellar growth. Moreover, a larger increase of the D_H was observed for the samples with
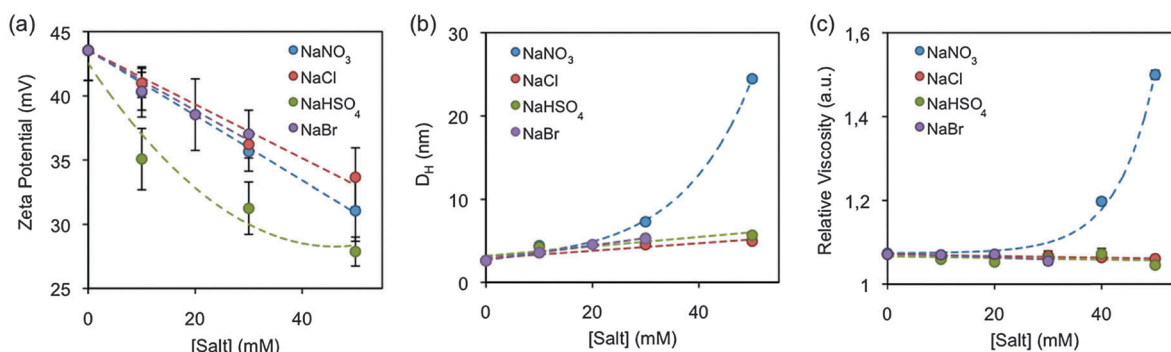

Fig. 5 (a) Zeta potential, (b) hydrodynamic diameter and (c) the relative viscosity of growth solutions in the presence of added Hofmeister salts.

This journal is © The Royal Society of Chemistry 2016

J. Mater. Chem. C, 2016, **4**, 53–61 | 57

[NaNO$_3$] > 30 mM. Such a kind of growth is related to the existence of interactions between the micelles, also called a semi-diluted regime.

In addition to the DLS measurements, the solution viscosity was also characterised. As soon as the micelle morphology changes from sphere to rod-like or worm-like, the micelles start entangling with each other (semi-dilute regime), subsequently the solution viscosity increases.[34] Fig. 5c plots the relative viscosity of growth solutions as a function of increasing salt content at 23 °C. Under the growth conditions, the viscosity is only affected by nitrate. Bromide, chloride and bisulphate do not show any significant effect. Interestingly, the viscosity starts increasing at NaNO$_3$ concentrations above 30 mM. Those are the same concentrations that also show a semi-dilute regime by DLS.

Finally, cryo-transmission electron microscopy (cryo-TEM) studies were performed to characterise the micelle morphology in the presence of NaNO$_3$, NaCl and NaHSO$_4$ (NaBr was excluded from the cryo-TEM study, because the bromide anion tunes the rod aspect ratio through a different mechanism, which will be described in the next section). The micelle shape has been hypothesized to play an important role in directing the Au NR growth.[20,49] Fig. 6a reveals mostly spherical CTAB micelles (97.9%) in the absence of additional Hofmeister salts, with a

small percentage of ellipsoidal micelles (2.1%). Interestingly, although the spherical shape is the most common in all the samples (Fig. 6b–g), the addition of salts increases the proportion of ellipsoidal (1.5 < AR < 3) and rod-like (AR > 3) micelles rather than the size of all micelles (Fig. 7), and these shape transitions increase the overall micelle size observed by DLS. Nevertheless, the micelle dimensions seem to slightly increase with the addition of salts (Table S5, ESI†), however the tendency is not as clear as the increase in the
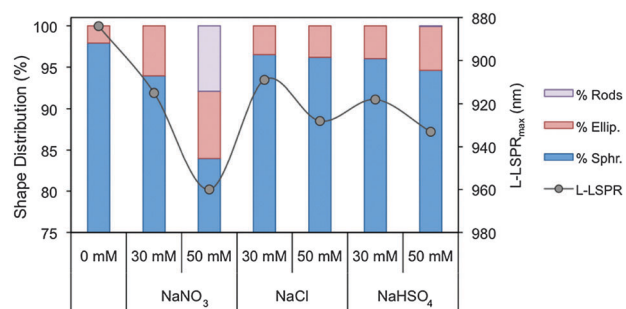

Fig. 7 Micelle shape distribution (spherical, ellipsoidal and rod-like micelles) in growth solutions at different Hofmeister salt concentrations and the L-LSPR$_{max}$ of the rods grown in those solutions.
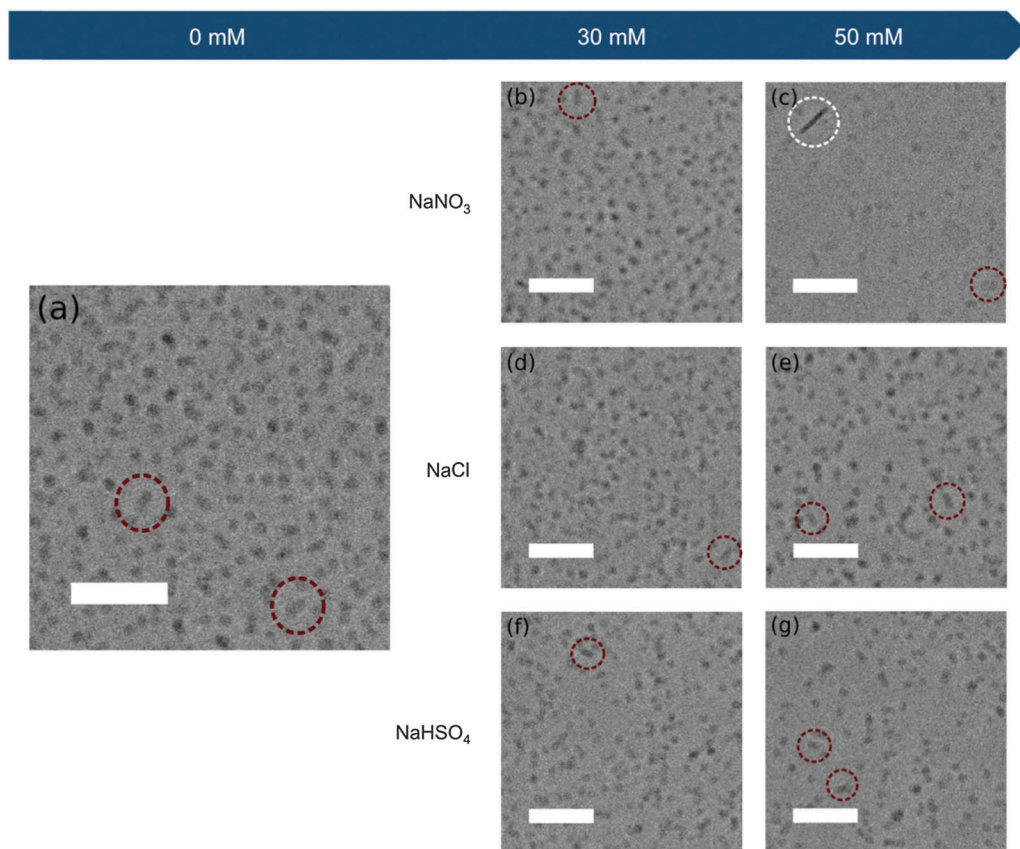

Fig. 6 Cryo-TEM images of CTAB micelles in the growth solutions with different amounts of Hofmeister salts: (a) without Hofmeister salts, (b and c) with NaNO$_3$, (d and e) with NaCl and (f and g) with NaHSO$_4$ in the order of increasing added concentration (30 and 50 mM). Some ellipsoidal and rod-like micelles have been highlighted in red and white dashed circles, respectively. All scale bars are 50 nm.

58 | *J. Mater. Chem. C*, 2016, **4**, 53–61

This journal is © The Royal Society of Chemistry 2016

number of non-spherical micelles. These results are in agreement with previously published studies, which show the co-existence of spherical and wormlike micelles in the same solution.[50] It is worth mentioning that the only solution visualised with rod-like micelles is the one with a $NaNO_3$ concentration of 50 mM. This is coherent with the semi-diluted regime observed by DLS and rheological measurements. It is important to note that the cryo-TEM images were taken from the growth solutions after the addition of the Hofmeister salts. As the growth of the Au NRs occurs, some ionic species such as Ag^+, $AuCl_4^-$ and ascorbate are consumed, in which ascorbate is added in the form of ascorbic acid in the second step. Therefore, the variation in their concentration might affect the CTAB micelles. Nevertheless, this seems quite unlikely since their concentrations are very low (i.e. the initial concentrations of silver nitrate, chloroauric acid and ascorbic acid are 0.1, 0.5 and 0.5 mM, respectively) and strong Hofmeister anions, such as nitrate, require a concentration of 10 mM to show a significant effect.

Growth mechanism

Despite the fact that silver-assisted Au NR synthesis was developed over a decade ago,[20] its mechanism is still very controversial and poorly understood. Currently, three main mechanisms have been proposed for the nanoparticle anisotropy: (1) silver is under-potentially deposited at specific gold crystal faces, preventing the crystal growth at those faces;[51,52] (2) the bromide–silver complex plays a role as a face-specific capping agent;[51,52] and (3) CTAB micelles act as soft templates.[20,49] All three mechanisms are supported by the experimental data, making it difficult to choose between the opposed theories. In a recent review,[53] Murphy et al. surveyed the current state of the art in the Au NR growth mechanism and suggest that the three mechanisms may be correct to some extent, the final mechanism being a combination of all three.

Our work provides a deeper understanding of the Au NR anisotropic growth and addresses some of the unanswered questions described before. In this section we list the most important observations obtained from our experimental data.

First of all, it is worth mentioning that few groups have previously reported the effect of salts on the growth of Au NRs with different results than ours. Mulvaney et al. reported the decrease of the aspect ratio after adding NaCl to the growth solution.[28] However, they synthesized penta-twinned Au NRs, which diverge from the single crystal Au NR in different ways, such as the structure and synthetic protocol (e.g. low CTAB concentration, 8 mM, and absence of $AgNO_3$). On the other hand, Yong et al. observed an increase of the aspect ratio at nitrate and chloride concentrations above 0.1 M.[49] Nevertheless, the rods obtained were highly polydisperse and presented significant shape impurities. That was probably due to the high concentration of salts in the growth solution, which may have induced wormlike micelles.[54,55]

Second, there seems to be a correlation between the decrease of the CTAB electric potential and the amount of shape impurities. The addition of Hofmeister salts decreased the zeta potential of CTAB micelles to different extents and increased

the shape impurities to a certain degree (Fig. S1, ESI†). $NaHSO_4$ induced the highest electrokinetic decrease, i.e. from 43.5 mV down to 27.9 mV, and yielded the highest amount of shape impurities, i.e. up to 13%. NaBr induced a significant amount of spherical nanoparticles too, i.e. up to 9%, however this can be accounted for by a different mechanism that will be described later. NaCl presents a highly variable amount of shape impurities and it is difficult to reach a solid conclusion. However the general impurity tendency is smaller than in the first salt. Finally, $NaNO_3$ is the salt that produces rods with higher shape purity. Even though the syntheses of penta-twinned and single crystal Au NRs follow different synthetic protocols, Mulvaney et al. reported a similar observation for the silverless synthesis, where the rod formation depends on the extremely strong binding between gold anions and cationic micelles.[28] Therefore, the decrease of the micelle zeta potential weakens the electrostatic interaction between the two species and may decrease the rod yield. In aromatic based synthesis,[29] where organic additives are introduced into the silver-assisted synthesis, the authors hypothesized that a weaker interaction between CTAB micelles and the gold pre-cursor yields shorter Au NRs. However, we did not observe such a phenomenon except for the bromide, whose case will be discussed later.

Third, some studies have suggested that under Au NR growth conditions,[20,49] CTAB micelles present rod-shaped morphology. Thus, the Au NR anisotropy would be driven by the micelle that acts as a soft template. To the best of our knowledge, this is the first work that has visualized the CTAB micelles under Au NR synthesis conditions by cryo-electron microscopy. The surfactant micelles were mostly spherical in all the cases, with an increasing amount of ellipsoidal micelles ($1.5 < AR < 3$) with the addition of salts. Only the sample with 50 mM $NaNO_3$ presented rod-like micelles ($AR > 3$), which were significantly smaller than the resulting Au NRs, 22.8×5.0 and 42.6×8.6 nm, respectively. Therefore, the soft template seems unlikely to form as it was proposed in those studies. Nevertheless, Murray et al. have recently suggested that the increase of the Au NR aspect ratio after the addition of organic additives is coherent with an increase of the surfactant packing parameter (p).[29] This phenomenon is also observed here, where the transition of spherical micelles ($p < 1/3$)[34] to ellipsoidal and rod-like micelles ($1/3 < p < 1/2$)[34] after the addition of the salts is consistent with the shift of L-LSPR$_{max}$ of AuNRs (Fig. 7). Thus, the change in the micellar behaviour, whether the surfactant molecule is directly bonded to the gold or to another surface (e.g. under-potentially deposited silver) or in the form of a different surface-active species (e.g. silver–CTAB complex), seems to affect the growth of the rod.

Fourth, the samples with NaBr presented a decrease in their aspect ratio and a blue-shift of the LSPR band proportional to the amount of salt, although the salt triggered the overall micellar growth. This anomalous behaviour can be explained by understanding the interaction between the bromide ions and gold. Halides are known to affect the growth of gold nanoparticles through two cooperative pathways.[56] (1) Halide

anions can complex with gold ion derivatives, modifying their potential and solubility, thereby altering their reduction rate.[57,58] The reduction potentials of $AuCl_2^-$, $AuBr_2^-$ and AuI_2^- are 1.154, 0.960 and 0.578 V, respectively.[59] The lower the standard reduction potential of a complex, the more difficult it is to be reduced by ascorbic acid. Additionally, the solubility of those complexes decreases in the order, $AuCl_2^- > AuBr_2^- > AuI_2^-$, and the formation of less soluble compounds slows down the reaction.[60] (2) Halides can also bind to the gold surface, blocking the growth of the nanoparticle. The binding strength of the halides increases in the following order $Cl^- < Br^- < I^-$.[61] In addition, Mirkin *et al.* reported that the passivation of the gold surface by halides further disturbs the silver under-potential deposition onto the gold surface.[56] This strong interference of halides with the Au NR growth has been observed for iodide, wherein low concentrations have been reported to reduce the aspect ratio of Au NRs and high concentrations to quench further and yield spherical nano-particles.[31,62] Therefore, the fact that bromide reduced the aspect ratio of the Au NRs can be explained from the gold–halide interaction point of view. Additionally, we observed a concentration threshold for bromide, *i.e.* 30 mM, like the one reported for iodide, wherein above that concentration the Au NR synthesis is completely quenched and spherical particles are mainly obtained. On the contrary, chloride has less capacity to block gold deposition and it did not hinder the growth of Au NRs at the experimental concentrations. Finally, nitrate and bisulphate have been reported displaying very low affinity for gold in comparison to halides,[61,63] which explains why they did not interfere with the nanoparticle growth.

Conclusions

We demonstrate that a high level of control over the rod dimensions and a widely tuneable L-LSPR band can be achieved by adding small amounts of Hofmeister salts in the seed-mediated synthesis of Au NRs. The nature of the tuning depends on the double interaction between the salts with gold and the salts with surfactant micelles. Salting-in ions, like thiocyanate and perchlorate, induce the surfactant precipita-tion and the quenching of the Au NR formation. Neutral and salting-out anions screen the electrostatic repulsion between the surfactant molecule heads, inducing changes in the micellar behaviour. When anions with low affinity for gold, like nitrate, bisulphate and chloride, are added their addition yields longer aspect ratio rods. However, anions with high affinity for gold, like bromide, reduce the gold deposition, producing shorter aspect ratio rods. Interestingly, CTAB micelles are mainly sphere-shaped in all solutions. The addition of salt increases the overall micelle size by increasing the non-spherical micelle population, although the spherical shape is still the predomi-nant one. Hence, these results provide not only a new strategy for the precise tuning of the optical properties and morphology of Au NRs, but also a deeper understanding of the anisotropic growth mechanism of the nanoparticles.

Notes and references

1 A. Guerrero-Martínez, M. Grzelczak and L. M. Liz-Marzán, *ACS Nano*, 2012, **6**, 3655–3662.

2 F. Hao, C. L. Nehl, J. H. Hafner and P. Nordlander, *Nano Lett.*, 2007, **7**, 729–732.

3 S. Nauert, A. Paul, Y. R. Zhen, D. Solis Jr, L. Vigderman, W. S. Chang, E. R. Zubarev, P. Nordlander and S. Link, *ACS Nano*, 2013, **8**, 572–580.

4 L. Vigderman and E. R. Zubarev, *Langmuir*, 2012, **28**, 9034–9040.

5 X. Huang, P. K. Jain, I. H. El-Sayed and M. A. El-Sayed, *Lasers Med. Sci.*, 2008, **23**, 217–228.

6 L. C. Kennedy, L. R. Bickford, N. A. Lewinski, A. J. Coughlin, Y. Hu, E. S. Day and R. A. Drezek, *Small*, 2011, **7**, 169–183.

7 X. Huang, S. Neretina and M. A. El-Sayed, *Adv. Mater.*, 2009, **21**, 4880–4910.

8 T. B. Huff, L. Tong, Y. Zhao, M. N. Hansen, J. X. Cheng and A. Wei, *Future Medicine*, 2007, **2**, 125–132.

9 A. M. Alkilany, L. B. Thompson, S. P. Boulos, P. N. Sisco and C. J. Murphy, *Adv. Drug Delivery Rev.*, 2012, **64**, 190–199.

10 P. K. Jain, X. Huang, I. H. El-Sayed and M. A. El-Sayed, *Acc. Chem. Res.*, 2008, **41**, 1578–1586.

11 C. Kim, C. Favazza and L. V. Wang, *Chem. Rev.*, 2010, **110**, 2756–2782.

12 A. S. Stender, K. Marchuk, C. Liu, S. Sander, M. W. Meyer, E. A. Smith and N. Fang, *Chem. Rev.*, 2013, **113**, 2469–2527.

13 H. Wang, T. B. Huff, D. A. Zweifel, W. He, P. S. Low, A. Wei and J. X. Cheng, *Proc. Natl. Acad. Sci. U. S. A.*, 2005, **102**, 15752–15756.

14 L. Vigderman, B. P. Khanal and E. R. Zubarev, *Adv. Mater.*, 2012, **24**, 4811–4841.

15 R. M. Pallares, S. L. Kong, T. H. Ru, N. T. K. Thanh, Y. Lu and X. Su, *Chem. Commun.*, 2015, **51**, 14524–14527.

16 M. E. Stewart, C. R. Anderton, L. B. Thompson, J. Maria, S. K. Gray, J. A. Rogers and R. G. Nuzzo, *Chem. Rev.*, 2008, **108**, 494–521.

17 S. K. Ghosh and T. Pal, *Chem. Rev.*, 2007, **107**, 4797–4862.

18 K. A. Willets and R. P. Van Duyne, *Annu. Rev. Phys. Chem.*, 2007, **58**, 267–297.

19 N. R. Jana, L. Gearheart and C. J. Murphy, *J. Phys. Chem. B*, 2001, **105**, 4065–4067.

60 | *J. Mater. Chem. C*, 2016, **4**, 53–61

This journal is © The Royal Society of Chemistry 2016

20 B. Nikoobakht and M. A. El-Sayed, *Chem. Mater.*, 2003, **15**, 1957–1962.

21 M. Liu and P. Guyot-Sionnest, *J. Phys. Chem. B*, 2005, **109**, 22192–22200.

22 N. R. Jana, L. Gearheart and C. J. Murphy, *Adv. Mater.*, 2001, **13**, 1389–1393.

23 J. Pérez-Juste, I. Pastoriza-Santos, L. M. Liz-Marzán and P. Mulvaney, *Coord. Chem. Rev.*, 2005, **249**, 1870–1901.

24 D. K. Smith and B. A. Korgel, *Langmuir*, 2008, **24**, 644–649.

25 S. E. Lohse, N. D. Burrows, L. Scarabelli, L. M. Liz-Marzán and C. J. Murphy, *Chem. Mater.*, 2013, **26**, 34–43.

26 S. Si, C. Leduc, M. H. Delville and B. Lounis, *ChemPhysChem*, 2012, **13**, 193–202.

27 K. C. Ng and W. Cheng, *Nanotechnology*, 2012, **23**, 105602.

28 J. Pérez-Juste, L. M. Liz-Marzan, S. Carnie, D. Y. Chan and P. Mulvaney, *Adv. Funct. Mater.*, 2004, **14**, 571–579.

29 X. Ye, L. Jin, H. Caglayan, J. Chen, G. Xing, C. Zheng and C. B. Murray, *ACS Nano*, 2012, **6**, 2804–2817.

30 L. Vigderman and E. R. Zubarev, *Chem. Mater.*, 2013, **25**, 1450–1457.

31 L. Zhang, K. Xia, Z. Lu, G. Li, J. Chen, Y. Deng and N. He, *Chem. Mater.*, 2014, **26**, 1794–1798.

32 X. Ye, Y. Gao, J. Chen, D. C. Reifsnyder, C. Zheng and C. B. Murray, *Nano Lett.*, 2013, **13**, 2163–2171.

33 X. Ye, C. Zheng, J. Chen, Y. Gao and C. B. Murray, *Nano Lett.*, 2013, **13**, 765–771.

34 C. A. Dreiss, *Soft Matter*, 2007, **3**, 956–970.

35 S. Kumar, A. Z. Naqvi and Kabir-ud-Din, *Langmuir*, 2000, **16**, 5252–5256.

36 L. Abezgauz, K. Kuperkar, P. A. Hassan, O. Ramon, P. Bahadur and D. Danino, *J. Colloid Interface Sci.*, 2010, **342**, 83–92.

37 M. G. Cacace, E. M. Landau and J. J. Ramsden, *Q. Rev. Biophys.*, 1997, **30**, 241–277.

38 X. C. Jiang and M. P. Pileni, *Colloids Surf., A*, 2005, **295**, 228–232.

39 T. Zhang, A. Jiang, J. H. Harrison and S. Chen, *J. Chem. Technol. Biotechnol.*, 2012, **87**, 1098–1103.

40 O. R. Miranda, N. R. Dollahon and T. S. Ahmadi, *Cryst. Growth Des.*, 2006, **6**, 2747–2753.

41 T. K. Sau and C. J. Murphy, *Langmuir*, 2004, **20**, 6414–6420.

42 R. C. Wadams, L. Fabris, R. A. Vaia and K. Park, *Chem. Mater.*, 2013, **25**, 4772–4780.

43 Y. Zhang and P. S. Cremer, *Curr. Opin. Chem. Biol.*, 2006, **10**, 658–663.

44 M. J. Nicol, C. A. Fleming and R. L. Paul, The Chemistry of Gold Extraction, in *The Extractive Metallurgy of Gold*, ed. G. G. Stanley, South African Institute of Mining and Metallurgy, Johannesburg, 1987, pp. 831–905.

45 A. L. Underwood and E. W. Anacker, *J. Colloid Interface Sci.*, 1987, **117**, 242–250.

46 A. B. Shah, S. T. Sivapalan, B. M. DeVetter, T. K. Yang, J. Wen, R. Bhargava, C. J. Murphy and J. M. Zuo, *Nano Lett.*, 2013, **13**, 1840–1846.

47 H. W. Wang, C. F. Shieh, H. Y. Chen, W. C. Shiu, B. Russo and G. Z. Cao, *Nanotechnology*, 2006, **17**, 2689–2694.

48 R. Kumar and S. R. Raghavan, *Soft Matter*, 2009, **5**, 797–803.

49 K. T. Yong, Y. Sahoo, M. T. Swihart, P. M. Schneeberger and P. N. Prasad, *Top. Catal.*, 2008, **47**, 49–60.

50 K. Kuperkar, L. Abezgauz, K. Prasad and P. Bahadur, *J. Surfactants Deterg.*, 2010, **13**, 293–303.

51 P. K. Jain, X. Huang, I. H. El-Sayed and M. A. El-Sayed, *Acc. Chem. Res.*, 2008, **41**, 1578–1586.

52 E. C. Dreaden, A. M. Alkilany, X. Huang, C. J. Murphy and M. A. El-Sayed, *Chem. Soc. Rev.*, 2012, **41**, 2740–2779.

53 S. E. Lohse and C. J. Murphy, *Chem. Mater.*, 2013, **25**, 1250–1261.

54 M. E. Helgeson, T. K. Hodgdon, E. W. Kaler and N. J. Wagner, *J. Colloid Interface Sci.*, 2010, **349**, 1–12.

55 K. Kuperkar, L. Abezgauz, D. Danino, G. Verma, P. A. Hassan, V. K. Aswal and P. Bahadur, *J. Colloid Interface Sci.*, 2008, **323**, 403–409.

56 M. R. Langille, M. L. Personick, J. Zhang and C. A. Mirkin, *J. Am. Chem. Soc.*, 2012, **134**, 14542–14554.

57 J. Rodríguez-Fernández, J. Pérez-Juste, P. Mulvaney and L. M. Liz-Marzán, *J. Phys. Chem. B*, 2005, **109**, 14257–14261.

58 M. Eguchi, D. Mitsui, H. L. Wu, R. Sato and T. Teranishi, *Langmuir*, 2012, **28**, 9021–9026.

59 A. J. Bard, R. Parsons and J. Jordan, *Standard Potentials in Aqueous Solution*, Marcel Dekker, New York, 1985.

60 L. Brown and T. Holme, *Chemistry for Engineering Students*, Brooks/Cole, Belmont, 2011.

61 O. M. Magnussen, *Chem. Rev.*, 2002, **102**, 679–726.

62 D. K. Smith, N. R. Miller and B. A. Korgel, *Langmuir*, 2009, **25**, 9518–9524.

63 J. P. Sylvestre, S. Poulin, A. V. Kabashin, E. Sacher, M. Meunier and J. H. Luong, *J. Phys. Chem. B*, 2004, **108**, 16864–16869.